Continuous-wave second-harmonic generation in sodium vapor

B. D. Sinclair and M. H. Dunn
Physics Department, University of St. Andrews, North Haugh, St. Andrews, Fife KY16 9SS, Scotland, United Kingdom
(Received 7 May 1986)

A high-resolution study of magnetic-field-induced second-harmonic generation in sodium vapor has been carried out with use of a single-frequency continuous-wave dye laser. Resonant enhancement was obtained by tuning the laser to the frequency of the $3S \rightarrow 4D$ two-photon transition of the sodium atom. Experimental and theoretical results are presented showing the variation of the power and polarization properties of the second-harmonic radiation as the laser is tuned across the two-photon resonance, and as the transverse magnetic field is varied.

I. INTRODUCTION

Second-order nonlinear processes such as second-harmonic generation are not allowed in atomic vapors, which are isotropic, unless some form of external symmetry breaking is involved.[1] The study of these processes in vapors is interesting, as the nonlinear medium then consists of isolated atoms with well-defined energy levels and selection rules. We have used a magnetic field to break the vapor's symmetry. This, combined with the use of a continuous-wave, single-frequency dye laser to provide the fundamental radiation, has permitted us to undertake a detailed study of the effect of selection rules and line-broadening processes on second-harmonic generation in sodium vapor.

Previous reports of second-harmonic generation (SHG) and sum or difference frequency mixing (SFM,DFM) in vapors may be classified into groups depending on the symmetry-breaking technique used.

(i) A static electric field has been applied across the focal region of the beam.[2–23] In this case, however, it is generally the third-order nonlinearity which is involved; it mixes the two pump photons with the zero-frequency electric field.

(ii) High-intensity laser pump pulses with transverse intensity gradients have been used to produce SHG.[24–35] Most reports suggest that the symmetry is broken by the production of quasistatic electric fields in the nonlinear medium by the high-power pulse, allowing a form of SHG similar to (i). True second-order processes in atomic vapors are forbidden by parity arguments in the dipole approximation, but are possible if a higher-order multipole transition is used; this is the case in the next two groups.

(iii) Two intersecting, noncollinear beams with orthogonal polarizations have been shown to produce a coherent electric quadrupole moment which oscillates at the sum or difference frequency through the second-order nonlinearity.[11,14,36–39]

(iv) A static transverse magnetic field has been applied to the focal region of a single beam.[24,37,38,40–45] With no magnetic field present, a two-photon absorption drives coherent quadrupole moments at the second-harmonic, sum or difference frequency, but these moments do not radiate into the forward direction. A transverse magnetic field mixes the magnetic sublevels of the system by the Zeeman effect, causing a rotation of the quadrupole moments thus allowing SHG, SFM, or DFM.

In all these processes strong enhancement of the nonlinear effect may occur if the frequencies of the laser fields are chosen to be close to single- or two-photon resonances in the nonlinear medium.

It is the last type of symmetry breaking listed above in which we are most interested. The first report of magnetic-field-induced three-wave mixing was by Flusberg *et al.*[40] who produced DFM in thallium vapor at 1.28 μm on the dipole-forbidden $6\,^2P_{3/2}-6\,^2P_{1/2}$ transition. Matsuoka *et al.*[41] were the first to report SHG by this means, using the $3\,^2S_{1/2}-3\,^2D$ two-photon transition in sodium for resonant enhancement. The same group has published further experimental and theoretical results using the same enhancing transition.[43,45] They observed that in intense magnetic fields the plane of polarization of the second harmonic was rotated, and the dependence of the second-harmonic power on the magnetic field strength changed from a square law at low fields to saturation at 0.1 T.

All previous investigators of this effect have used pulsed lasers with large linewidths as the source of the fundamental field. Our group was the first to report continuous-wave, single-frequency, magnetic-field-induced second-harmonic generation.[44] This allows a detailed exploration of the nonlinear properties of the medium as the laser is tuned into resonance with an allowed two-photon transition. We have extended this work, and report here the first experimental and theoretical observations, to our knowledge, of properties of the SHG process which change across the line profile of the resonantly enhancing two-photon transition.[46]

Sodium vapor was used as the nonlinear medium. Enhancement of the process was obtained by tuning the laser into resonance with the $3S$-$4D$ two-photon transition at 578.7 nm. Parametric emission of the second-harmonic (SH) radiation occurred in the presence of the symmetry-breaking magnetic field by means of a coherent quadrupole emission at twice the laser frequency.

In Sec. II we develop the theoretical treatment of Uchiki, Nakatsuka, and Matsuoka[45] (UNM) by distinguishing between homogeneous and inhomogeneous line-

broadening processes, and by considering the special case of single-frequency fundamental radiation. This allows us to obtain expressions for the power and polarization of the SH beam as functions of the laser frequency, the magnetic field strength and the power and polarization angle of the fundamental light. The results of the theoretical model and the experimental studies are compared in Sec. III.

II. THEORY

Our analysis of second-harmonic generation in sodium vapor in a magnetic field follows that of UNM.[45] The system is considered to consist of three levels, s, p, and d, corresponding to the $3S$ ground states, the $3P$ intermediate states, and the resonantly enhancing $4D$ excited states of the sodium atom. In order to predict properties of the process which change across the line profile we use eigenstates of the Hamiltonian, $\mathscr{H}_0$, which include fine, hyperfine, and Zeeman splitting terms. These levels are shown in Fig. 1. We extend the theory presented by UNM by distinguishing between the homogeneous and inhomogeneous line-broadening processes. The homogeneous linewidth enters the analysis as a damping constant in the two-photon-induced coherence between the $3S$ and $4D$ states. The inhomogeneous (Doppler) linewidth is taken into account by integrating the equations for the induced quadrupole moment across the Maxwellian velocity distribution of the sodium atoms, with appropriately shifted atomic resonant frequencies.

The expectation value of the quadrupole moment oscillating at the second-harmonic frequency can be derived by consideration of the time evolution of the density operator ρ.[47] We define γ_{ii} to be the relaxation rate for the population in level i, and γ_{ij} $(i\neq j)$ to be the rate at which ρ_{ij} relaxes to zero. Then

$$\frac{\partial\rho_{ij}}{\partial t}=\frac{-i}{\hbar}[\mathscr{H},\rho]_{ij}-\gamma_{ij}(\rho-\bar{\rho})_{ij}\ , \tag{1}$$

where

$$\mathscr{H}=\mathscr{H}_0+\mathscr{H}_1\ , \tag{2}$$

$$\mathscr{H}_1=-\mathbf{p}\cdot\mathbf{E}=V\exp(-i\omega t)+\text{c.c.}\ , \tag{3}$$

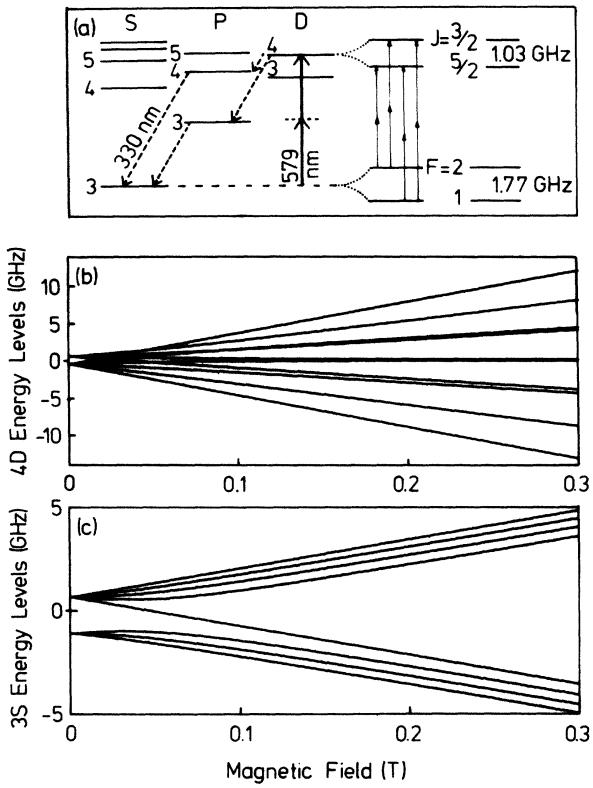

FIG. 1. Energy levels of the sodium atom, and the variation of the energies of the $4D$ and $3S$ levels in a magnetic field.

and

$$\bar{\rho}=\exp(-\mathscr{H}_0/k_BT)/\operatorname{tr}[\exp(-\mathscr{H}_0/k_BT)]\ . \tag{4}$$

$\mathscr{H}_1$ is the electric dipole interaction energy between the fundamental laser field $E=\epsilon\exp(-i\omega t)+\text{c.c.}$ and the atomic system, where ϵ and ω are the amplitude and frequency of the fundamental field, respectively. By use of second-order perturbation theory UNM showed that the expression for the slowly varying amplitude of the quadrupole moment Q_q is given by

$$\langle\tilde{Q}_q\rangle=\sum_{d,s}\int_{-\infty}^{t}\frac{\exp[i(2\omega-\omega_{ds}+i\gamma_{ds})(t-t')]T_q\rho_{ss}dt'}{i\hbar^2\langle\omega-\omega_{ps}+i\gamma_{ps}\rangle}\ , \tag{5}$$

where

$$T_q=\sum_p V_{dp}V_{ps}(Q_q)_{sd}\ , \tag{6}$$

and V_{ij} and $(Q_q)_{ij}$ are the dipole and quadrupole matrix elements, respectively, connecting states i and j; $\hbar\omega_{is}(J_i,m_i,F,m_F,H)$ is the energy separation of these states. H is the magnetic field strength. The summation is taken over all $3S$ and $4D$ states. T_q is the quantity which contains the selection rules of the process. This derivation is based on the assumptions that with no perturbation present only the diagonal elements of the ground states are nonzero, that the excitation is sufficiently weak for second-order perturbation theory to be applicable, and that the populations of the ground states are altered negligibly. The intermediate P states are assumed to be far off resonance; in the case we consider, the energy difference between the P states and the fundamental radi-

ation is 300 cm^{-1}, which is much greater than the spread of the P states under the conditions of interest.

We define the y axis as the direction of propagation of the fundamental laser beam, so the second-harmonic wave is driven by the effective dipole

$$(P_x,P_z)=-i\,|\,k_2\,|\,(Q_{xy},Q_{zy})/2\ . \tag{7}$$

If the magnetic field is applied parallel to the z axis, the components of the effective dipole are obtained[45] using Eq. (7) from

$$\tilde{Q}_{xy}=-\sum_{\substack{F,m_F,\\ J_d,m_d}}\int_{-\infty}^{t}\frac{\exp[i(2\omega-\omega_{ds}+i\gamma_{ds})(t-t')](B_2-B_{-2})}{20\sqrt{3}\hbar^2\langle\omega-\omega_{ps}+i\gamma_{ps}\rangle}\epsilon_x^2e^2r_{dp}r_{ps}Q_{sd}\rho_{ss}dt'\ , \tag{8}$$

$$\tilde{Q}_{zy}=-\sum_{\substack{F,m_F,\\ J_d,m_d}}\int_{-\infty}^{t}\frac{\exp[i(2\omega-\omega_{ds}+i\gamma_{ds})(t-t')]2(B_1-B_{-1})}{20\sqrt{3}\hbar^2\langle\omega-\omega_{ps}+i\gamma_{ps}\rangle}\epsilon_x\epsilon_ze^2r_{dp}r_{ps}Q_{sd}\rho_{ss}dt'\ , \tag{9}$$

where r_{ij} is the reduced dipole matrix element connecting states i and j, and Q_{sd} is the reduced quadrupole matrix element connecting the $4D$ and $3S$ states. The geometry of the system is now included only in the laser polarization and the B_q terms; the latter terms are given by

$$\begin{aligned}B_q(J_d,m_d,F,m_F,H)&=D_A^2(J_d,m_d,H)S_A^2(F,m_F,H)\delta(m_d-0.5+q)\\&\quad+D_B^2(J_d,m_d,H)S_B^2(F,m_F,H)\delta(m_d+0.5+q)\ .\end{aligned} \tag{10}$$

D_A and D_B are the expansion coefficients for each eigenstate of the $4D$ levels into the $m_s=\pm\frac{1}{2}$ basis states, and similarly S_A and S_B are the expansion coefficients for the $3S$ ground state with hyperfine quantum number F and magnetic quantum number m_F. Expressions for these magnetic-field-dependent quantities have been published by UNM.

In our experiments we used a single-mode, linearly polarized continuous-wave laser, the field of which may be described as

$$(\epsilon_x,\epsilon_z)=\epsilon_0\exp(-i\omega t)(\sin\theta,\cos\theta)+\text{c.c.}, \tag{11}$$

where θ is the angle between the plane of polarization of the laser and the z axis. In this case the integrals in Eqs. (8) and (9) are readily calculated to give

$$\tilde{Q}_{xy}=\frac{-iK\epsilon_x^2}{\langle\omega_{ps}-\omega-i\gamma_{ps}\rangle}\sum_{\substack{F,m_F,\\ J_d,m_d}}\frac{B_2-B_{-2}}{(\omega_{ds}-2\omega-i\gamma_{ds})}\ , \tag{12}$$

$$\tilde{Q}_{zy}=\frac{-iK\epsilon_x\epsilon_z}{\langle\omega_{ps}-\omega-i\gamma_{ps}\rangle}\sum_{\substack{F,m_F,\\ J_d,m_d}}\frac{2(B_1-B_{-1})}{(\omega_{ds}-2\omega-i\gamma_{ds})}\ , \tag{13}$$

where

$$K=\frac{e^2r_{dp}r_{ps}Q_{sd}\rho_{ss}}{20\sqrt{3}\hbar^2}\ . \tag{14}$$

We take into account the thermal motion of the atoms by including the effect of the Doppler shift in these equations.[38,47] The angular transition frequency of an atom moving with velocity v_y along the direction connecting the observer and the atom is

$$\omega_{ds}=\omega_{ds0}+kv_y\ , \tag{15}$$

where ω_{ds0} is the resonant angular frequency of an atom at rest relative to the observer and $k=2\pi/\lambda$. The Maxwellian velocity distribution function for a gas with atomic mass M at an absolute temperature T is

$$f(v_y)=[(M/2\pi k_BT)]^{1/2}\exp(-mv_y^2/2k_BT)\ , \tag{16}$$

where k_B is Boltzmann's constant. Equations (12) and (13) are therefore modified to the form

$$\tilde{Q}_{xy}=\frac{-iK\epsilon_x^2[(M/2\pi k_BT)]^{1/2}}{\langle\omega_{ps}-\omega-i\gamma_{ps}\rangle}\times\sum_{\substack{F,m_F,\\ J_d,m_d}}\int_{-\infty}^{\infty}\frac{(B_2-B_{-2})\exp(-mv_y^2/2k_BT)dv_y}{(\omega_{ds}+kv_y-2\omega-i\gamma_{ds})}\ , \tag{17}$$

$$=\frac{-iK\epsilon_x^2}{\langle\omega_{ps}-\omega-i\gamma_{ps}\rangle\Omega}\times\sum_{\substack{F,m_F,\\ J_d,m_d}}(B_2-B_{-2})Z[(2\omega-\omega_{ds}+i\gamma_{ds})/\Omega]\ , \tag{18}$$

where

$$\Omega=2\omega(2k_BT/mc^2)^{1/2} \tag{19}$$

is the Doppler width of the second-harmonic radiation, and $Z(a+ib)$ is the plasma dispersion function

$$Z(a+ib)=\pi^{-0.5}\int_{-\infty}^{\infty}\frac{\exp(-t^2)dt}{t-(a+ib)}\ . \tag{20}$$

We calculate the required values of $Z(a+ib)$ by numerical integration of the complex differential equation which defines the plasma dispersion function.[48] These values, together with the expressions for the energy levels and wave-function components given in UNM, allow us to

calculate the values of $\tilde{Q}_{xy}$ and $\tilde{Q}_{zy}$. As we are concerned with the $4D$ states rather than the $3D$ states we use a value of -411.2 MHz for the magnitude of the spin perturbation in the Zeeman effect on these states.

The intensity of the second-harmonic radiation is given by

$$I_{\mathrm{SH}} \propto \tilde{Q}_{xy}\tilde{Q}^{*}_{xy} + \tilde{Q}_{zy}\tilde{Q}^{*}_{zy} \ . \tag{21}$$

The second-harmonic light is, in general, elliptically polarized. Its polarization state is specified by the orientation of the ellipse axes, and their lengths a and b $(a > b)$. We give the latter information in terms of the second-harmonic power, and the eccentricity[49] of the ellipse,

$$\eta = (a-b)/a \ . \tag{22}$$

If the radiation is examined through an analyzer which has its transmission axis at θ_A to the z axis, the intensity of the detected signal is given by

$$I_{\mathrm{SH}}(\theta_A) \propto |\, \tilde{Q}_{xy} \sin\theta_A + \tilde{Q}_{zy} \cos\theta_A \,|^2 \ . \tag{23}$$

The value of θ_A which gives the maximum value of $I_{\mathrm{SH}}(\theta_A)$ is

$$\theta_{A\,\max} = 0.5 \tan^{-1}\left[\frac{\tilde{Q}_{xy}\tilde{Q}^{*}_{zy} + \tilde{Q}^{*}_{xy}\tilde{Q}_{zy}}{|\tilde{Q}_{zy}|^2 - |\tilde{Q}_{xy}|^2} \right] \ . \tag{24}$$

This corresponds to the angle between the z axis and the major axis of the ellipse describing the light. The eccentricity of the light can then be obtained from

$$\eta = 1 - [I_{\mathrm{SH}}(\theta_{A\,\max} + 90°)/I_{\mathrm{SH}}(\theta_{A\,\max})]^{1/2} \ . \tag{25}$$

If no magnetic field is present,

$$B_2(J_d, m_d, F, m_F, 0) = B_{-2}(J_d, -m_d, F, -m_F, 0)$$

and

$$\omega_{ds}(J_d, m_d, F, m_F, 0) = \omega_{ds}(J_d, -m_d, F, -m_F, 0) \ ;$$

this leads to a zero result for the sum in Eq. (17) which gives $\tilde{Q}_{xy}$, and so no effective dipole for SHG exists in the x direction. A similar argument holds for the effective dipole in the z direction. When a transverse magnetic field is applied to the vapor, Zeeman splitting breaks these equalities and so SHG is then possible.

The B_j terms are dependent on the magnetic field strength but not the laser frequency. They describe the mixing of the magnetic quantum level eigenfunctions by the magnetic field, as the field is increased from zero, through the low-field Zeeman effect, and into the Paschen-Back and Back-Goudsmit regions. There is little change in their values above 0.1 T.

The resonant denominators, however, are dependent on both the magnetic field strength and the laser frequency. The contribution to the resonant enhancement of the SHG made by any transition depends on its detuning from the SH frequency, and hence on the magnetic field through Zeeman splitting.

At low fields $\tilde{Q}_{xy}$ and $\tilde{Q}_{zy}$ are both proportional to the magnetic field strength; this causes the second-harmonic intensity to be proportional to the square of the magnetic field strength, and the second harmonic to have the same linear polarization as the fundamental. At higher fields the two quadrupole moments of interest grow at different rates, causing a rotation of the polarization of the second harmonic. The real and imaginary parts of each moment also have different dependencies on the magnetic field strength, which results in a phase difference between the two effective dipoles, and hence a deviation from linear polarization of the second-harmonic light.

III. RESULTS

We chose sodium vapor as our nonlinear medium and used the $3S$-$4D$ transition at 578.7 nm to enhance resonantly the magnetic-field-induced second-harmonic generation. The energy levels of the sodium atom are well known, and the two-photon absorption lies within the tuning range of Rhodamine 6G dye lasers. Some relevant levels of this atom are shown in Fig. 1. The vapor was produced in a heat pipe oven[50] operated at 300 °C with 1 mbar of argon buffer gas. The length of the vapor zone was 10 cm.

The fundamental light source was a ring dye laser (Spectra Physics 380D) which produced up to 500 mW of continuous-wave, single-frequency light with a linewidth of less than 0.5 MHz, when pumped with an argon ion laser. The polarization properties of the light entering the oven were controlled by an out-of-plane three-mirror system and/or a Soleil-Babinet compensator. The light was focused into the center of the oven by a 20 cm focal-length lens.

A. Doppler-free calibration techniques

The experimental arrangement is shown in Fig. 2. The collision broadened linewidth of the $3S$-$4D$ transitions was measured by Doppler-free two-photon spectroscopy. A linear polarizer and quarter-wave plate were used to produce circularly polarized light and to prevent feedback into the laser from the reflected beam. A 12.7 cm focal-length quartz lens and a dichroic plane mirror were used to retroreflect the laser light and to focus the spontaneous ultraviolet fluorescence, which monitored the population of the $4D$ state, on to a filtered photomultiplier tube (Hamamatsu R212 with two Corning 9863 filters). No magnetic fields were applied. Four peaks in the uv signal

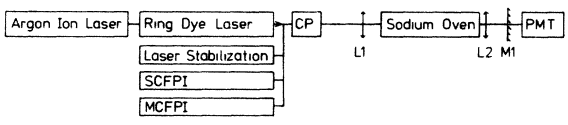

FIG. 2. Schematic diagram of the experimental arrangement used for two-photon spectroscopy: SCFPI, scanning confocal Fabry-Perot interferometer; MCFPI, marker confocal Fabry-Perot interferometer, which had a 250 MHz free spectral range; CP, circular polarizer; $L1$, 20-cm focal-length lens; $L2$ 12.7-cm focal-length quartz lens; $M1$, plane dichroic mirror (highly reflecting in the visible, highly transmitting in the ultraviolet). PMT, filtered photomultiplier tube.

were obtained as expected,[51] due to the hyperfine splitting of the $3S$ state and the fine splitting of the $4D$ state. The width of the peaks was limited by pressure broadening; the half width at half maximum was used as the value for γ_{ds} in the theoretical model. A small discrepancy may arise here, as the quantity measured was γ_{dd} rather than γ_{ds} required by the theory. However, it was found that none of the observable quantities was predicted to vary rapidly with γ_{ds} around the 35 MHz value measured and used in the calculations. An increase in γ_{ds} is expected to cause a decrease in the SH power, as it is essentially a damping term, though the effect is not large until γ_{ds} is of the order of the Doppler width.

We used the peak corresponding to the $3S(F=2) \rightarrow 4D(J=\frac{3}{2})$ transition to give us an absolute frequency calibration of the laser with respect to the atomic transition; we call this frequency f_0. The laser was then detuned from this peak by a known amount by monitoring the transmission of a thermally stabilized confocal interferometer, which had a free spectral range of 250 MHz and was also used as a frequency marker.

B. Second-harmonic generation study

A similar experimental arrangement was used as for the Doppler-free work, but the quarter-wave plate was removed so that the fundamental light was linearly polarized, and dichroic mirror $M1$ was now offset so that it was acting merely as a filter to discriminate against the fundamental light. Two arrangements were used to detect the SH. For most experiments it was detected directly using a narrow passband system consisting of a filtered solar blind photomultiplier tube (Hamamatsu R166UH with two Corning 9863 filters); this arrangement was insensitive to the other dominant uv radiation that was present. However, when comparing the line profiles of the SH and the 330-nm radiation, the SH was passed through a 1-m monochromator and detected by the same filtered photomultiplier tube as the 330-nm radiation. A dc magnetic field of up to 0.3 T was applied perpendicular to the laser beam across the center of the cell. For most of these experiments phase-sensitive detection was used to improve the signal-to-noise ratio.

1. Phase mismatching effects

A relatively low field of 0.06 T was applied across the oven and the laser was tuned to the peak of the SHG profile, corresponding to the frequency at which the $3S$-$4D$ transition provided the strongest resonant enhancement of the SHG. The polarization of the SH light was perpendicular to the magnetic field. The SH light was detected by a filtered solar blind photomultiplier tube. The temperature of the oven was slowly varied to change the sodium particle density, which was calculated from the formula quoted by Miles and Harris.[52]

As long as the fundamental and second-harmonic stay in phase during their propagation through the sodium vapor a squared dependence on the particle density is expected for this type of coherent process.[44] This is seen to be the case experimentally for calculated densities up to 2×10^{14} cm^{-3} as shown in Fig. 3. At higher densities an

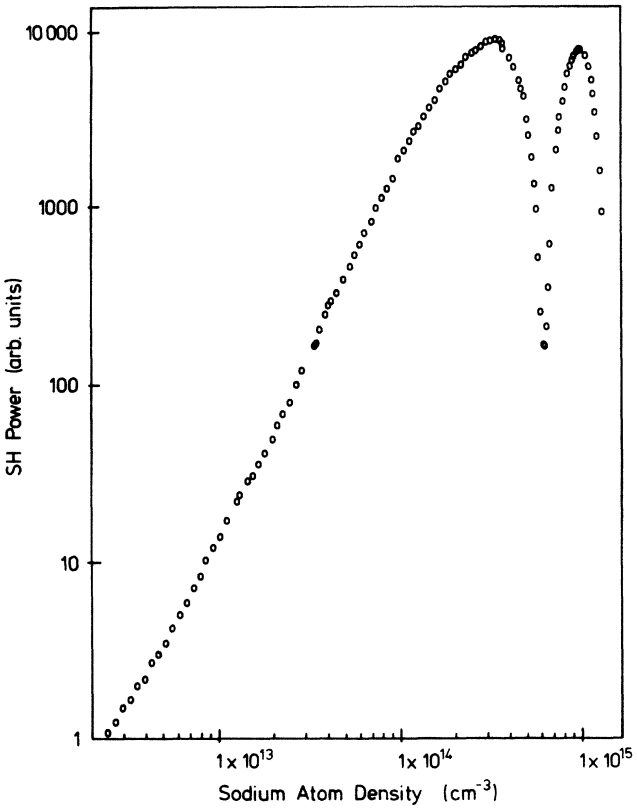

FIG. 3. Measured variation of the second-harmonic power with sodium particle density.

oscillatory behavior of the SH power was observed. This is characteristic of a phase mismatch occurring between the fundamental and second-harmonic waves. The change in the phase velocity between the two frequencies is due to dispersive effects in the vapor, caused largely by the strong $3S$-$3P$ resonance lines affecting the refractive index at the fundamental frequency. These effects may be calculated using the Sellmeier equations.[52] The first peak in the second-harmonic power is expected at a particle density of 3.5×10^{14} cm^{-3}; close to the observed value of 3.4×10^{14} cm^{-3}. The small discrepancy may be due to dispersion on the $3S$-$4D$ quadrupole resonance, and the presence of sodium dimers. In other experiments we have observed ten peaks in the SH power as the particle density was increased; the peak heights decreased with particle density due to the associated increases in the Doppler width and the pressure broadening term. With a 0.1 T magnetic field applied across the oven, which was operated at a temperature corresponding to the first peak of Fig. 3, and a fundamental power of 120 mW, the second-harmonic power was measured to be 7 nW.

To minimize problems of phase mismatching, all the following experiments were carried out at 300°C, corresponding to a particle density of 2.3×10^{14} cm^{-3}.

2. Line profiles

The variation in the second-harmonic power as the laser was tuned through the resonantly enhancing two-photon

transition was examined experimentally using the laser system described above. The polarization of the fundamental beam was arranged to be at 90° to the field, and the SH radiation produced in the oven was detected by a filtered solar blind photomultiplier tube. The signals from this and the photodiode monitoring the transmission of the marker interferometer were recorded on a computer. This allowed subsequent compensation for the slightly nonlinear laser frequency scan by using a simple algorithm to linearize the data. Sets of curves such as those in Fig. 4(a) were produced; each curve in this figure corresponds to a different magnetic field strength, and the same scale was used for each one. A set of theoretically calculated curves, based on a temperature of 300 °C and a γ_{ds} of 35 MHz, is shown in Fig. 4(b). It can be seen from these figures that when the Zeeman splitting is comparable to the Doppler width, there is no further increase in peak SH power with magnetic field. The satisfactory agreement between theoretically predicted and experimentally observed profiles is a clear demonstration of the successful role of atomic selection rules in modeling this nonlinear process.

The line profile of the two-photon absorption with different magnetic fields was also measured experimentally. In these cases the spontaneous fluorescence at 330 nm was passed through a monochromator and detected by a filtered photomultiplier tube. The same arrangement was also used to detect the SH signal, but the monochromator was set to transmit light at 289 nm. The shapes of the line profiles obtained at 0.021 and 0.3 T are shown in Fig. 5. The second-harmonic profile in the former case is seen to be similar to, but slightly narrower than, the line profile of the enhancing $3S$-$4D$ transition. At higher magnetic fields, when the Zeeman splitting exceeds the Doppler width, the relative contributions of the different magnetic sublevels change significantly across the line profile, and this results in the structure seen on both the fluorescence and SHG curves in Fig. 5(b). The marked difference between the two profiles is due to the different selection rules in the two cases. In high magnetic fields two photons of x-polarized fundamental radiation connect the $m_l=0$ ground states with the $m_l=0,\pm2$ $4D$ states, thus giving rise to the three peaks in the 330-nm fluorescence. Since it is only those connections involving the $m_l=\pm2$ $4D$ states that contribute to the quadrupole tensor, only the two outer peaks are seen in the SHG line profile. We believe that this is the first direct observation of the difference between the selection rules in second-harmonic generation and in resonant two-photon absorption.

In both graphs the theoretically calculated SHG line

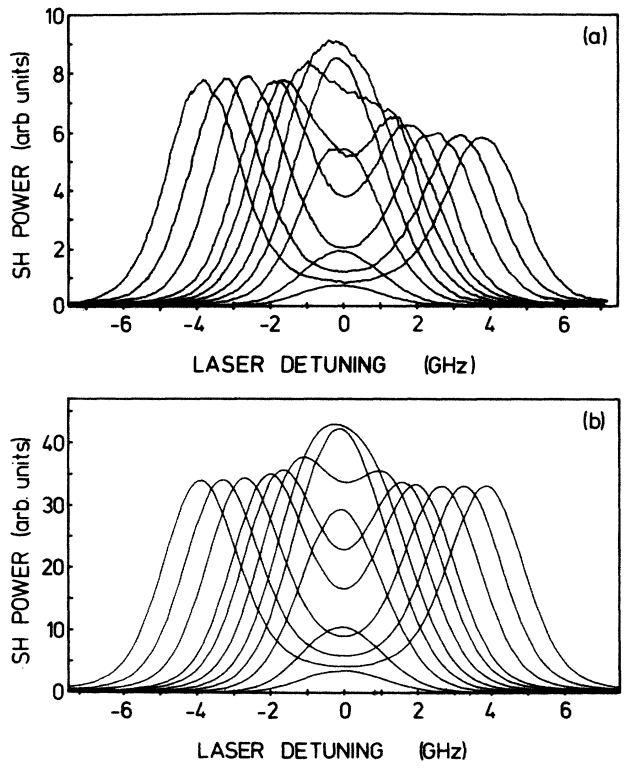

FIG. 4. (a) Experimentally and (b) theoretically obtained variation of the second-harmonic power with laser frequency, as the laser was tuned through the enhancing $3S$-$4D$ two-photon transition, at different magnetic field strengths: 0.016 T (the curve with the lowest maximum), 0.028, 0.052, 0.074, 0.096, 0.121, 0.147, 0.167, 0.210, 0.250, and 0.290 T (the widest curve). The magnetic field was perpendicular to the laser polarization.

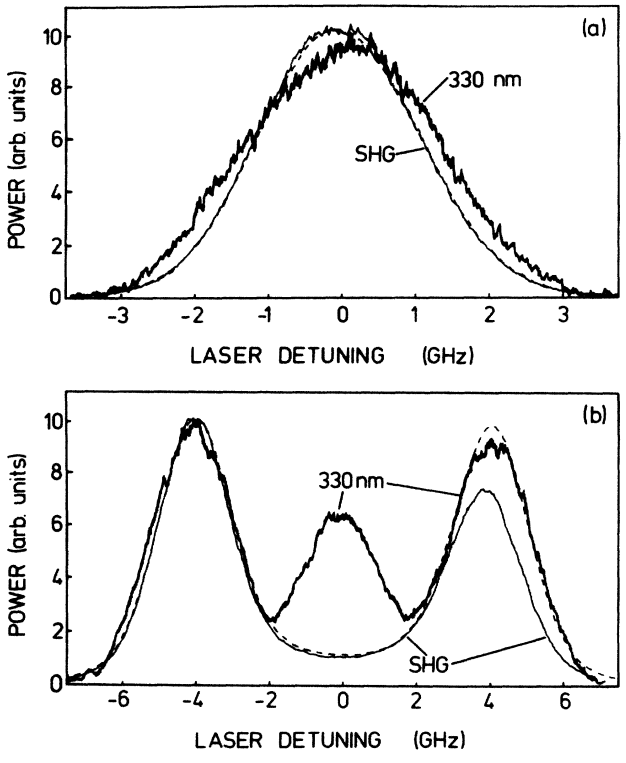

FIG. 5. Line profiles as the laser was tuned across the $3S$-$4D$ two photon resonance (a) at 0.021 T and (b) at 0.30 T, with the laser polarization set at 90° to the magnetic field. The dashed line is the theoretically calculated curve for the second-harmonic generation, the narrow solid line is the experimentally determined second-harmonic generation (SHG) line profile, and the thicker solid line is the line profile of the 330-nm radiation which was used to monitor the population of the $4D$ states.

profile is shown as a broken line. Agreement is very good at 0.021 T, and over much of the line profile at 0.3 T. The asymmetry of the experimentally obtained curve is not expected to such a degree from our model. We are investigating the origin of this difference; it is probably due to bulk effects in the medium, such as phase mismatching.

To excite both effective dipoles simultaneously, the fundamental polarization was set at 45° to the magnetic field. The line profiles of the radiation emanating from the two effective dipoles were measured separately by inserting an appropriately orientated linear polarizer into the SH beam. At a low field the line profiles are similar, as shown in Fig. 6(a). At a higher field of 0.294 T the magnitudes and splittings of the line profiles are significantly different, as seen in Fig. 6(b). Equation (10) shows that different transitions drive the two effective dipoles. The Q_{xy} moment involves only those $4D$ states which have $m_l = \pm 2$, whereas the Q_{zy} moment involves only those with $m_l = \pm 1$. Hence the differences can most readily be seen at high fields when Zeeman splittings are large and m_l approximates to a good quantum number. The Q_{xy} profile shows about twice the splitting of the Q_{zy} profile due to these differences in selection rules. The polarizer was removed from the SH beam so that radiation from both effective dipoles contributed to the SH line profiles, as shown in Fig. 7. These line profiles are considerably different from those in Fig. 4 as the Q_{zy} quadrupole moment is now also contributing to the SHG process.

3. *Variation of the power and polarization of the second harmonic with magnetic field*

The laser polarization was set at 45° to the magnetic field so that both effective dipoles were excited. The power and polarization properties of the SH were examined as the magnetic field strength was varied, at a constant laser frequency. The SH power was measured using a filtered solar blind photomultiplier tube. The polarization properties of the SH light were measured in two distinct ways. In the first, a linear polarizer was inserted between the oven and the detector. The polarizer was rotated to the positions of minimum and maximum SH signal; the angle of the polarizer gave the polarization angle of the SH, and the square root of the ratio of the signal strengths at the two positions gave the ratio of the lengths of the ellipse axes. A second, "null," method was devised to measure a/b, in order to avoid problems due to the nonuniform response of the photomultiplier tube. A Soleil-Babinet compensator was set up as a quarter-wave

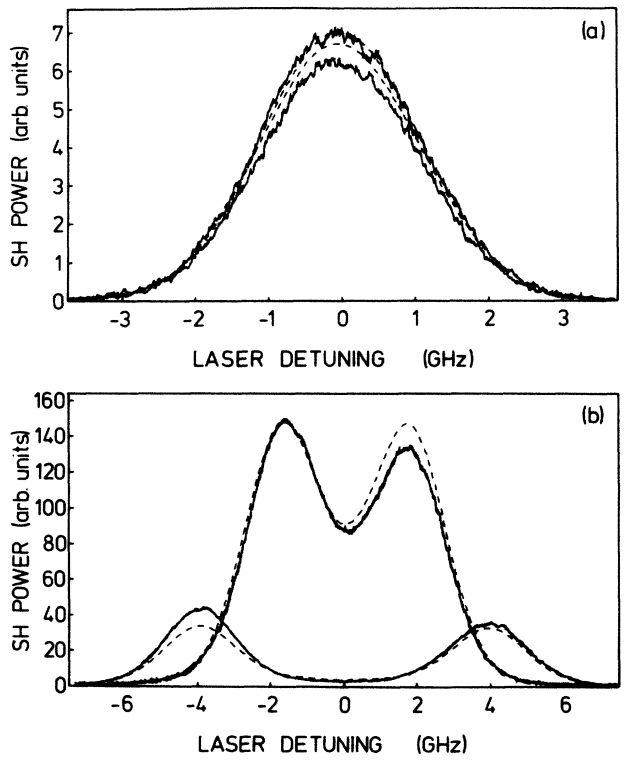

FIG. 6. Line profiles of the second-harmonic radiation emanating from the two effective dipoles (a) at 0.022 T and (b) at 0.294 T, with the laser polarization set at 45° to the magnetic field. The solid lines are experimentally determined, the dashed lines are theoretically calculated. The curves with the greater maximum in each case were produced by the z effective dipole, the other by the x effective dipole.

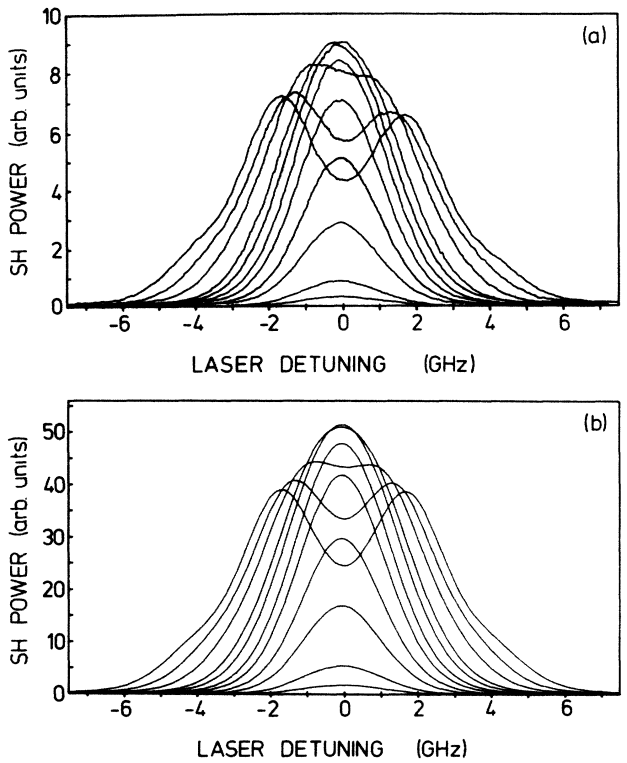

FIG. 7. Line profiles of the second harmonic with the fundamental radiation at 45° to the magnetic field. The curves in (a) are experimentally obtained, those in (b) are theoretically calculated. The different curves are at different magnetic field strengths: 0.016 T (the curve with the lowest maximum), 0.028, 0.052, 0.074, 0.100, 0.120, 0.147, 0.168, 0.212, 0.250, and 0.290 T (the widest curve).

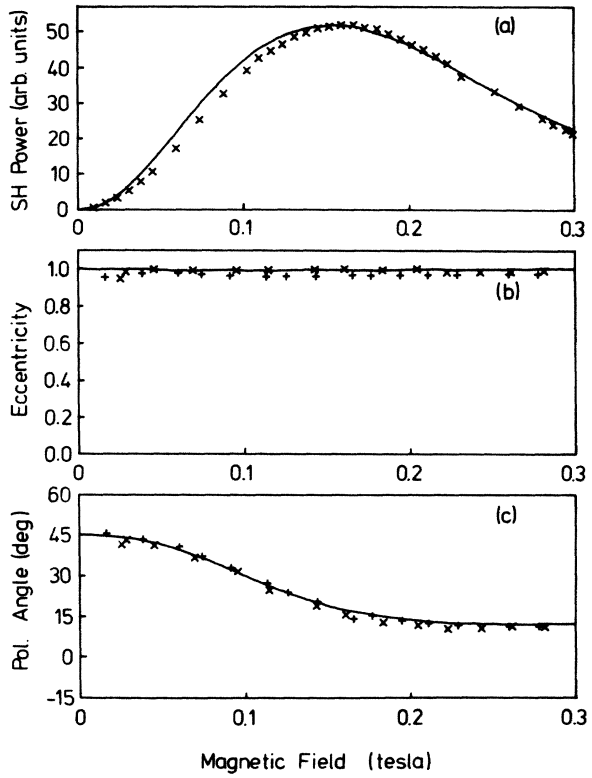

FIG. 8. Power and polarization properties of the second-harmonic radiation as functions of the magnetic field strength. The field was at 45° to the polarization of the fundamental, and the laser was tuned to f_0 (approximately the line center of the $3S$-$4D$ two-photon transition). The experimental points in (b) and (c) were taken in the two ways described in the text: + using the polarizer alone, × using the null technique. The curves are theoretically calculated; the curve in part (a) was normalized to have the same maximum value as the experimental readings. The calculations assumed a vapor temperature of 300 °C and a damping constant γ_{ds} of 35 MHz.

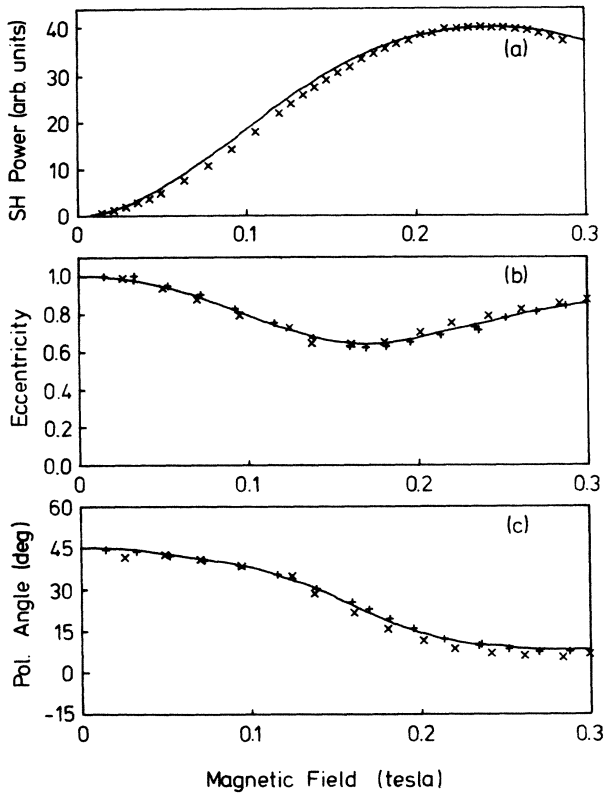

FIG. 9. Power and polarization properties of the second-harmonic radiation as functions of the magnetic field strength, at a laser frequency of $f_0+1.5$ GHz. Other conditions were the same as those listed with Fig. 8.

plate at 289.3 nm and was inserted in the SH beam with a linear polarizer between it and the detector. Zero SH signal was obtained only if the axes of the quarter-wave plate were along the axes of the polarization ellipse, and if the transmission axis of the polarizer was at 90° to the linearly polarized light created by the quarter-wave plate. The orientation of the ellipse was then given directly by the angular position of the quarter-wave plate, and the ratio of the lengths of the ellipse axes was given by the tangent of the angle between the quarter-wave plate and the linear polarizer.

The power and polarization properties of the SH were investigated at three laser frequencies: f_0, $f_0+1.5$ GHz, and f_0+3 GHz. The strikingly different results obtained at these three frequencies are shown in Figs. 8, 9, and 10. In all cases there is good agreement between the theoretically predicted behavior, which is shown by solid lines, and the experimental readings marked as points on the graphs.

At f_0, which is approximately at the center of the Doppler-broadened two-photon absorption peak, the SH power is seen [Fig. 8(a)] to rise to a peak at 0.16 T, as can also be deduced from Fig. 7. The eccentricity of the SH is very close to one (i.e., the polarization of the SH is almost linear) at all fields as seen in Fig. 8(b). This is due to the two effective dipoles being almost exactly in phase with each other at all field strengths; the maximum expected phase difference between them is calculated to be 1.3°. Because of the different growth rate of the two effective dipoles, the polarization of the SH rotates as the field is increased, as shown in Fig. 8(c).

Figure 11 shows the theoretically calculated size and relative phase of the two effective dipoles when the laser is tuned to f_0+3 GHz; a damping constant of 35 MHz and a vapor temperature of 300 °C were used in the calculation. At this laser frequency, the peak in the magnitude of the x effective dipole occurs at 0.23 T, as is seen experimentally in Fig. 4. At this field and frequency the transitions which contribute to Q_{xy} are Zeeman shifted to cause maximum resonant enhancement. Because the transitions which drive Q_{zy} are subject to less relative Zeeman splitting than those driving Q_{xy}, the size of the former moment is seen to be still increasing at 0.3 T, as the Zeeman effect moves the appropriate level differences closer into resonance with the SH frequency. The sum of the SH power due to the two moments shown in Figs. 11(a) and 11(b) gives the total SH power shown in Fig. 10(a). Fig-

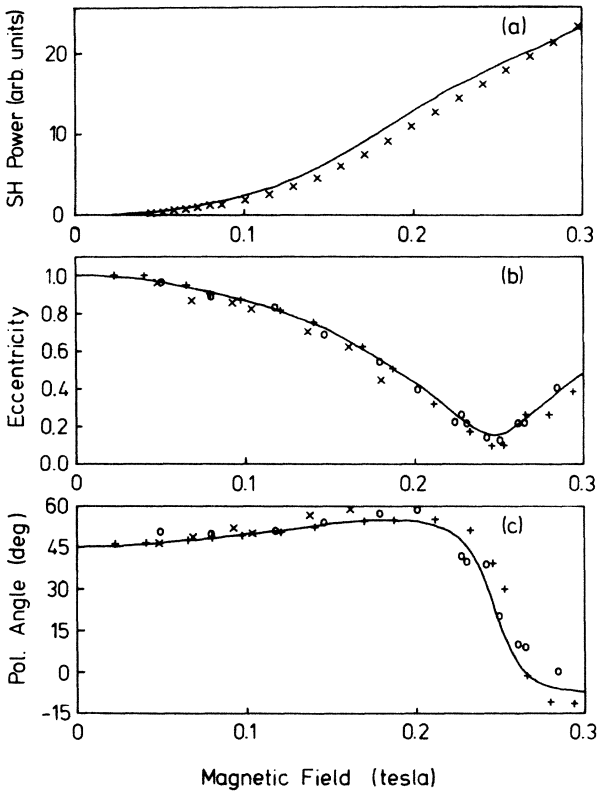

FIG. 10. Power and polarization properties of the second-harmonic radiation as functions of the magnetic field strength, at a laser frequency of f_0+3 GHz. Other conditions were the same as those listed with Fig. 8, but the circles mark another set of experimental results taken using the null method.

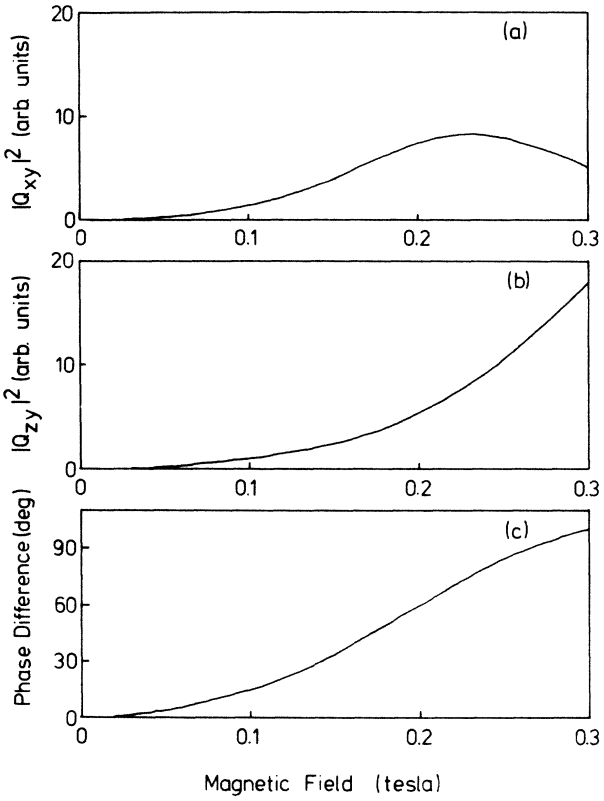

FIG. 11. Calculated magnitudes of, and phase difference between, the two effective dipoles driving the second-harmonic radiation. These are plotted as functions of the magnetic field strength, at a laser frequency of f_0+3 GHz. A vapor temperature of 300 °C, and a damping constant γ_{ds} of 35 MHz were assumed.

ures 8(a) and 9(a) show peaks in the SH power; as these results were taken closer to line center, a smaller field was required to shift the appropriate levels into positions of maximum resonant enhancement, and the size of the x and z effective dipoles have passed their maxima by 0.3 T.

The calculated phase difference between the two effective dipoles at the laser frequency f_0+3 GHz is shown in Fig. 11(c) as a function of magnetic field. The maximum phase difference at this laser frequency is much greater than at f_0. The relative phase of the two moments affects the polarization state of the SH radiation. This is seen in Fig. 10(b) as a reduction in the eccentricity of the SH, though circularly polarized light is not produced, as the two moments have different magnitudes. However, a phase difference of greater than 90° would result in the polarization angle passing into the next quadrant; Fig. 10(c) and 11(c) show this happening at 0.26 T.

At low fields, the major contribution to the variation in the magnitudes of the quadrupole moments comes from the variation of the B_j terms, rather than from the change in the values of the denominators in Eq. (17). In this case of small Zeeman splitting, the two effective dipoles have approximately the same strength and phase, so the SH is linearly polarized in the same direction as the fundamental field. As the relative phases and sizes of the effective dipoles change, due to major differences between the values of the resonant denominators applying to the two quadrupole moments, large deviations from linear polarization and rotation of the polarization angle are observed. Closer to line center, these effects are less pronounced, as shown in Figs. 8 and 9.

4. *Second-harmonic power dependence on the fundamental polarization*

In order to measure the dependence of the second-harmonic power on the fundamental polarization angle, a half-wave plate was inserted before the oven to vary the angle between the plane of polarization of the fundamental and the magnetic field. The SH power was measured directly by a filtered solar blind photomultiplier tube.

At low fields, in which the two effective dipoles grow at the same rate when the fundamental polarization is at 45° to the magnetic field, the SH power is expected to show a $\sin^2\theta$ dependence on the polarization angle θ. This was observed and is shown in Fig. 12. The difference in the growth rate of the two effective dipoles in higher magnetic fields was described in Sec. III B 3. This leads to a more complicated relationship between the fundamental polarization angle and the SH power. At a fundamental polarization angle of 90° only the x effective dipole is driven, and the SH power appropriate to that dipole alone

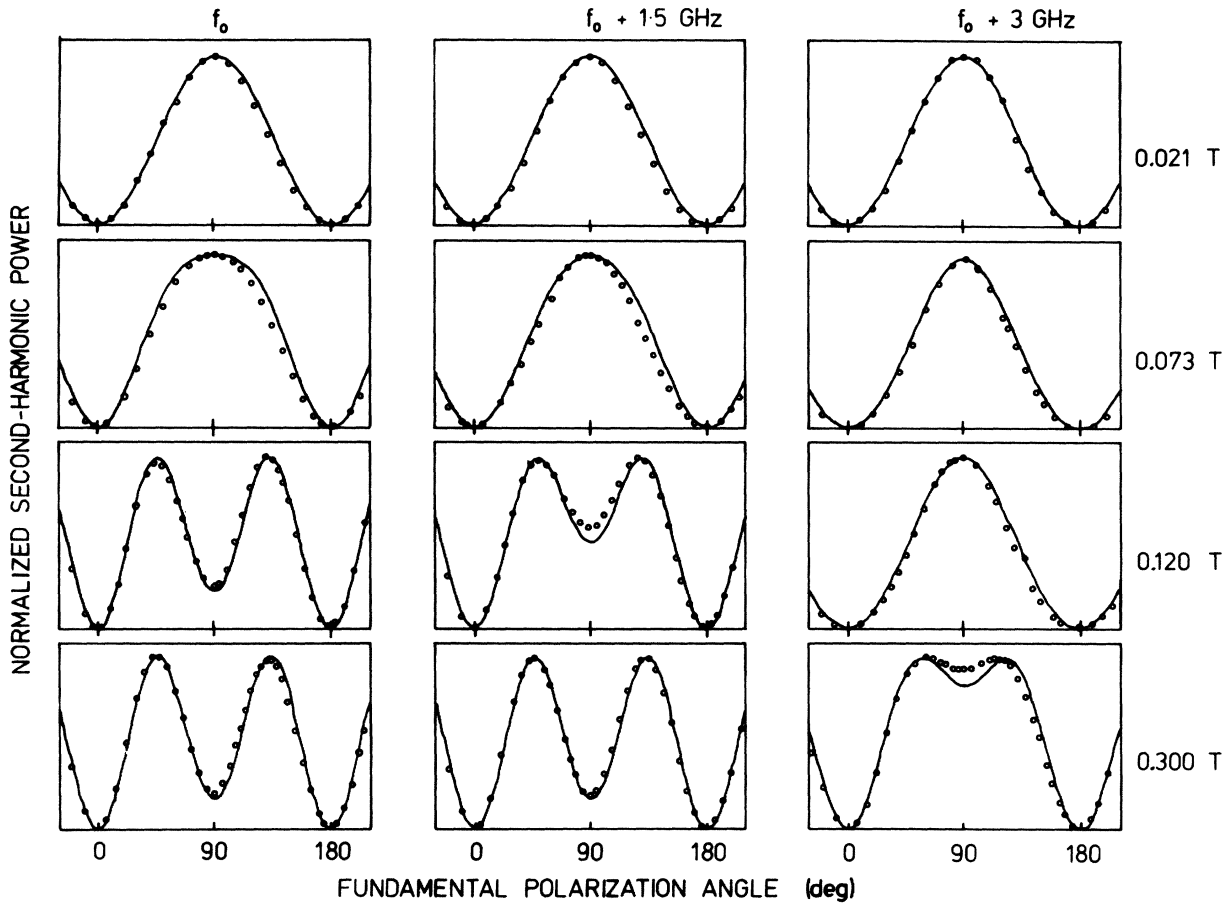

FIG. 12. Variation of second-harmonic power with the fundamental polarization angle. Each theoretically calculated curve was normalized to have the same peak power as its associated set of experimental results. Columns 1 to 3 show the results for the laser tuned to f_0, $f_0+1.5$ GHz, and f_0+3 GHz, respectively. The different rows show the results for different magnetic field strengths.

is obtained. At other angles the z effective dipole is also driven, and it adds to the total SH power. This effective dipole is strongest at angles of 45° and 135°. Figure 12 shows that the theory and experiment agree that the maximum deviation from the $\sin^2\theta$ behavior occurs at the highest magnetic fields and closest to line center.

IV. CONCLUSIONS

The theoretical treatment described in Sec. II has been shown to predict well the results of the experimental investigation of continuous-wave, single-frequency second-harmonic generation induced in sodium vapor by the application of a transverse magnetic field.

The model developed includes the role played by the atomic selection rules associated with the different magnetic sublevels, and the effects of homogeneous and inhomogeneous broadening. It successfully predicts the variation of the power and polarization properties of the second-harmonic radiation with the laser frequency, the magnetic field strength, and the polarization angle of the fundamental radiation. These dependences are interpreted in terms of the interaction between two perpendicular effective dipoles radiating at the second-harmonic frequency, the relative magnitudes and phases of which change with magnetic field strength and laser frequency. We obtained considerably better agreement between experiment and theory when we modeled the homogeneous and inhomogeneous atomic line-broadening processes separately, instead of just using a damping constant related to the Doppler width.[45,46]

By using a single-frequency laser and an atomic nonlinear medium, we believe that we are the first to examine experimentally the properties of a SHG process in such detail, providing a stringent test of the model developed to predict the basic properties of the nonlinear effect in terms of fundamental atomic parameters.

Significant changes occur in the shape of the modeled curves as the Doppler width is altered, and as the damping constant is increased to a significant fraction of the Doppler width. We are currently investigating these effects experimentally.

ACKNOWLEDGMENTS

This work was supported by the Science and Engineering Research Council Grant No. GR/D 38651. One of us (B.D.S.) gratefully acknowledges personal financial support from the Science and Engineering Research Council.

[1]N. Bloembergen, *Nonlinear Optics* (Benjamin, New York, 1965).
[2]G. Mayer, C. R. Acad. Sci. Ser. B **267**, 54 (1968).
[3]S. Kielich, IEEE J. Quantum Electron. **QE-5**, 562 (1969).
[4]R. S. Finn and J. F. Ward, Phys. Rev. Lett. **26**, 285 (1971).
[5]I. J. Bigio and J. F. Ward, Phys. Rev. A **9**, 35 (1974).
[6]R. S. Finn and J. F. Ward, J. Chem. Phys. **60**, 454 (1974).
[7]J. F. Ward and I. J. Bigio, Phys. Rev. A **11**, 60 (1975).
[8]I. J. Bigio, R. S. Finn, and J. F. Ward, Appl. Opt. **14**, 336 (1975).
[9]G. M. Krochik and Yu. G. Khronupolo, Sov. J. Quantum Electron. **4**, 1076 (1975).
[10]J. K. Guha, Appl. Opt. **15**, 2381 (1976).
[11]D. S. Bethune, R. W. Smith, and Y. R. Shen, Phys. Rev. Lett. **38**, 647 (1977).
[12]R. L. Abrams, A. Yariv, and P. A. Yeh, IEEE J. Quantum Electron. **QE-13**, 79 (1977); R. L. Abrams, C. K. Asawa, T. K. Plant, and A. E. Popa, *ibid.* **QE-13**, 82 (1977).
[13]C. K. Miller and J. F. Ward, Phys. Rev. A **16**, 1179 (1977).
[14]D. S. Bethune, R. W. Smith, and Y. R. Shen, in *Coherence and Quantum Optics IV,* edited by L. Mandel and E. Wolf (Plenum, New York, 1978).
[15]J. W. Dudley and J. F. Ward, Appl. Opt. **20**, 1777 (1981).
[16]R. W. Boyd and L. Xiang, IEEE J. Quantum Electron. **QE-18**, 1242 (1982).
[17]Y. T. Lam and T. Thirunamachandran, J. Chem. Phys. **77**, 3810 (1982).
[18]D. P. Shelton and A. D. Buckingham, Phys. Rev. A **26**, 2787 (1982).
[19]D. J. Gauthier, J. Krasinsky, and R. W. Boyd, Opt. Lett. **8**, 211 (1983); R. W. Boyd, D. J. Gauthier, I. Krasinski, and M. S. Malcuit, IEEE J. Quantum Electron. **QE—20**, 1074 (1984).
[20]V. Mizrahi and D. P. Shelton, Phys. Rev. A **31**, 3145 (1985).
[21]V. Mizrahi and D. P. Shelton, Phys. Rev. Lett. **55**, 696 (1985).
[22]V. Mizrahi and D. P. Shelton, Phys. Rev. A **32**, 3454 (1985).
[23]D. P. Shelton and V. Mizrahi, Phys. Rev. A **33**, 72 (1986).
[24]T. Mossberg, A. Flusberg, and S. R. Hartman, Opt. Commun. **25**, 121 (1978).
[25]K. Miyazaki, T. Sato, and H. Kashiwagi, Phys. Rev. Lett. **43**, 1154 (1979).
[26]J. Heinrich and W. Behmenburg, Appl. Phys. **23**, 333 (1980).
[27]K. Miyazaki, T. Sato, and H. Kashiwagi, Phys. Rev. A **23**, 1358 (1981).
[28]J. Okada, Y. Fukuda, and M. Matsuoka, J. Phys. Soc. Jpn. **50**, 1301 (1981).
[29]V. G. Arkhipkin *et al.,* Sov. J. Quantum Electron. **11**, 656 (1981).
[30]D. S. Bethune, Phys. Rev. A **23**, 3139 (1981).
[31]D. S. Bethune, Phys. Rev. A **25**, 2845(E) (1982).
[32]R. R. Freeman, J. E. Bjorkholm, R. Panock, and W. E. Cooke, in *Laser Spectroscopy V,* edited by A. R. W. McKellar, T. Oka, and B. P. Stoicheff (Springer-Verlag, Berlin, 1981).
[33]V. G. Arkhipkin *et al.,* Opt. Quantum Electron. **13**, 436 (1981).
[34]W. Jamroz, P. E. Larocque, and B. P. Stoicheff, Opt. Lett. **7**, 148 (1982).
[35]V. Mizrahi and D. P. Shelton, Phys. Rev. A **33**, 1396 (1986).
[36]D. S. Bethune, R. W. Smith, and Y. R. Shen, Phys. Rev. Lett. **37**, 431 (1976).
[37]A. Flusberg, T. Mossberg, and S. R. Hartman, Phys. Rev. Lett. **38**, 694 (1977).
[38]D. S. Bethune, R. W. Smith, and Y. R. Shen, Phys. Rev. A **17**, 277 (1978).
[39]D. S. Bethune, Opt. Lett. **6**, 287 (1981).
[40]A. Flusberg, T. Mossberg, and S. R. Hartman, Phys. Rev. Lett. **38**, 59 (1977).
[41]M. Matsuoka, H. Nakatsuka, H. Uchiki, and M. Mitsunaga, Phys. Rev. Lett. **38**, 894 (1977).
[42]A. Flusberg, T. Mossberg, and S. R. Hartman, in *Coherence and Quantum Optics IV,* edited by L. Mandel and E. Wolf (Plenum, New York, 1978).
[43]H. Uchiki, H. Nakatsuka, and M. Matsuoka, Opt. Commun. **30**, 345 (1979).
[44]M. H. Dunn, Opt. Commun. **45**, 346 (1983).
[45]H. Uchiki, H. Nakatsuka, and M. Matsuoka, J. Phys. Soc. Jpn. **52**, 3010 (1983).
[46]Some of these results were presented by us at the 1986 International Quantum Electronics Conference; B. D. Sinclair and M. H. Dunn, in IQEC '86 Technical Digest, San Francisco 1986, (unpublished), p. 120.
[47]A. Yariv, *Quantum Electronics* (Wiley, New York, 1975).
[48]B. D. Fried and S. D. Conte, *The Plasma Dispersion Function, The Hilbert Transform of the Gaussian* (Academic, New York, 1961).
[49]S. G. Lipson and H. Lipson, *Optical Physics* (Cambridge University Press, London, 1969).
[50]C. R. Vidal and J. Cooper, J. Appl. Phys. **40**, 3370 (1969).
[51]T. W. Hansch, K. C. Harvey, G. Meisel, and A. L. Schawlow, Opt. Commun. **11**, 50 (1974).
[52]R. B. Miles and S. E. Harris, IEEE J. Quantum Electron. **QE-9**, 470 (1973).